中国光学（中英文）
Chinese Optics
核心期刊

A novel high-precision refractive index measurement scheme based on entangled coherent states and parity detection

HAO Li-li, SONG Pu, LIU Xiao-yan, YANG Xiao-hao, WANG Qiang

Citation:
HAO Li-li, SONG Pu, LIU Xiao-yan, YANG Xiao-hao, WANG Qiang. A novel high−precision refractive index measurement scheme based on entangled coherent states and parity detection[J]. *Chinese Optics*, In press. doi: 10.37188/CO.EN−2026−0002
郝利丽, 宋甫, 刘孝研, 杨晓豪, 王强. 基于纠缠相干态和奇偶探测的高精度折射率测量新方法[J]. 中国光学, 优先发表. doi: 10.37188/CO.EN−2026−0002

View online: https://doi.org/10.37188/CO.EN−2026−0002

文章编号　2097-1842(xxxx)x-0001-10

A novel high-precision refractive index measurement scheme based on entangled coherent states and parity detection

HAO Li-li, SONG Pu, LIU Xiao-yan, YANG Xiao-hao, WANG Qiang*
(*School of Physics and Electronic Engineering*, *Northeast Petroleum University*, *Daqing* 163318, *China*)
* *Corresponding author*, *E-mail*: *wangqiang*8035@163.*com*

Abstract: Traditional intensity-based refractive index measurement methods are constrained by the classical diffraction limit and the shot noise limit, which severely restricts the improvement of measurement precision. To address this issue, a novel quantum measurement scheme integrating entangled coherent states (ECS) and parity detection (PD) is proposed. Taking advantage of the non-classical correlation of quantum entanglement, the scheme constructs a dual-mode entangled coherent state light source and realizes high-fidelity signal demodulation through a customized parity detection system. Theoretical derivation and numerical simulation results demonstrate that the measurement resolution of the proposed scheme breaks through the Rayleigh limit, achieving a $\sqrt{N}$-fold improvement compared with the traditional coherent state measurement method in the full loss range. In lossless scenarios and cases with loss rates below 10%, the sensitivity surpasses the shot noise limit. Finally, the experimental challenges faced by the experiment are also elaborated in detail. This quantum measurement architecture provides a new technical pathway for precision optical detection, biosensing, and other fields, exhibiting significant practical value and broad application prospects.
Key words: refractive index measurements; entangled coherent states; parity detection; super-resolution; ultra-sensitivity

基于纠缠相干态和奇偶探测的高精度折射率测量新方法

郝利丽, 宋　甫, 刘孝研, 杨晓豪, 王　强*
（东北石油大学 物理与电子工程学院, 黑龙江 大庆 163318）

摘要: 传统基于强度探测的折射率测量方法受经典衍射极限与散粒噪声极限的制约, 限制了测量精度的进一步提升。本文提出一种纠缠相干态结合奇偶探测方法的折射率测量新方案。该方案利用量子纠缠的非经典关联特性, 构建双模纠缠相干态光源, 通过奇偶探测手段实现信号的高性能测量。理论推导与数值仿真结果表明, 所提方案的测量分辨率突破瑞利极限, 在全损耗区域内相较于传统相干态测量方法, 分辨率提升 $\sqrt{N}$倍, 在无损耗及损耗率低于 10% 的场景下, 灵敏度超越散粒噪声极限。最后, 对实验所面临的挑战进行了详细说明。该量子测量架构为精密光学检测、生物传感等领域提供了新的技术路径, 具有显著的实用价值与广阔的应用前景。
关　键　词: 折射率测量; 纠缠相干态; 奇偶探测; 超分辨率; 超灵敏度

收稿日期: 2026-01-06; **修订日期:** xxxx-xx-xx

中图分类号:O431 文献标志码:A doi:10.37188/CO.EN-2026-0002 CSTR:32171.14.CO.EN-2026-0002

1 Introduction

The refractive index is a fundamental parameter characterizing the optical properties of materials, and its measurement accuracy plays a crucial role in advancing technologies in materials science, biomedicine, precision manufacturing, and other fields. The measurement and control of refractive index can realize beam manipulation[1], study the electronic and magnetic properties of materials[2-3] and identify the composition and concentration of solutions[4]. With the development of photolithography and micromachining technology in recent years, refractive index measurement instruments can be seamlessly connected to computers or other devices to realize automated measurement and control[5-6].

The traditional high-precision refractive index measurement methods are mainly depending on the wave optics[7] which focuses on using interference, diffraction and polarization[8] of light. Such as fiber optic ball lens interferometer[9], grating diffraction method[10], double polarization photonic crystal fiber sensing method, line array CCD automatic measurement method[11] and so on. The resolution and sensitivity based on diffraction and polarization methods are limited by the range of the detected refractive index. In addition, the experimental repeatability is poor, the instrument adjustment is complicated and the measurement work is heavy. The interferometric method can realize the measurement accuracy of 10^{-6}[12] and is theoretically not limited by the refractive index range. However, the complex structure and optical path make the interferometric strategy difficult to popularize its application. What is worse, the existing refractive index detecting methods are ultimately based on intensity detection (ID), and the resolution and sensitivity of ID is limited by the refractive index measurement Rayleigh diffraction limit (RDL) and shot noise limit (SNL)[13], the detection performances are difficult to be further improved.

To overcome the constraints of classical physical limits, quantum optical technologies have emerged as a promising solution for refractive index measurement. Quantum entanglement, as a core resource, can enhance the sensitivity and resolution of measurement systems through non-local correlation properties, and has demonstrated significant advantages in phase sensing, displacement measurement, and other applications[14-15]. Among existing quantum measurement schemes, interferometric methods based on entangled photon pairs can break through the shot noise limit[16]. However, the entangled photon pairs state is a discrete-variable (DV) entangled state, methods using entangled photon pairs (e.g., Bell states) require SPDC sources, which have low photon generation efficiency (<1 photon pair per pump pulse) and require precise alignment of pump lasers and nonlinear crystals. Additionally, DV systems often need single-photon detectors and quantum memory to maintain entanglement, increasing resource complexity and cost.

In recent years, entangled coherent states (ECS) have attracted increasing attention in the field of quantum sensing due to their high entanglement degree[17]. ECS is a continuous-variable (CV) quantum state generated from coherent states (macroscopic photon ensembles, N>>1) via linear optical elements (beam splitters, phase shifters). This avoids the need for complex single-photon sources (e.g., SPDCs) or quantum dot emitters, which are resource-intensive to fabricate and operate. For example, generating ECS with N requires only two coherent lasers and a 50/50 beam splitter—resources that are standard in most optical labs. According to Ref. [17], ECS also has better loss resistance. However, DV systems are highly vulnerable to loss. Even a 10% loss can reduce entanglement fidelity by >50% (per existing literature [16, 18]), as single-photon loss directly breaks the entanglement correlation.

To tackle the aforementioned issues, this paper proposes a novel refractive index measurement scheme based on the combination of entangled coherent states and parity detection[19-20]. By optimizing the quantum state preparation and detection process, the scheme achieves resolution breakthrough in the full loss range and sensitivity enhancement in low-loss scenarios. This paper elaborates on the theoretical foundation, simulation design, and performance verification of the scheme, providing theoretical and practical support for the development of high-precision refractive index measurement technologies.

2 Measurement principle and scheme design

2.1 Physical nature of classical measurement limits

The performance bottleneck of traditional intensity-based measurement methods stems from two core physical limits. Firstly, the Rayleigh limit, determined by the wave nature of light, essentially limits the spatial resolution due to diffraction effects during photon propagation, which is mathematically expressed as $\lambda/2$ (where λ is the incident light wavelength). Secondly, the shot noise limit, caused by the statistical fluctuation of photon counting, has a sensitivity upper bound of $1/\sqrt{N}$ (where N is the number of detected photons). These two limits collectively form the performance ceiling of classical measurement technologies, which cannot be fundamentally broken through by optimizing optical system parameters.

2.2 Overall Scheme Architecture

The core architecture of the proposed scheme consists of three parts: an entangled coherent state light source, a refractive index sensing module, and a parity detection system, with the specific structure illustrated in Fig. 1.

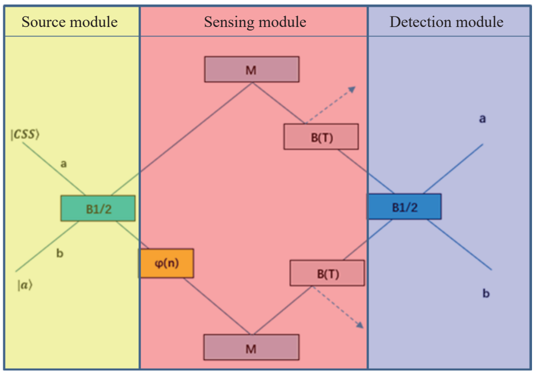

Fig. 1 Schematic representation of the refractive index measurement system.

图 1 折射率测量系统结构示意图

In this setup, the counterclockwise light path, designated as "a," serves as the signal path, while the clockwise light path, marked as "b," functions as the reference path. The coherent superposition states $|CSS\rangle = N_\alpha\left(\left|\alpha/\sqrt{2}\right\rangle + \left|-\alpha/\sqrt{2}\right\rangle\right)$ and the coherent states $|CS\rangle = \left|\alpha/\sqrt{2}\right\rangle$ are introduced into ports a and b, respectively, where $N_\alpha = \left[2\left(1+e^{-|\alpha|^2}\right)\right]^{-1/2}$ and $\alpha = \sqrt{N}$. These states subsequently interfere at the initial 50-50 beam splitter $\hat{B}_{1/2}$, resulting in the generation of entangled coherent states $|ECS\rangle = N_\alpha(|\alpha\rangle_a|0\rangle_b + |0\rangle_a|\alpha\rangle_b)$. As the light traverses the sensing path a, it accumulates a phase shift $\varphi(n) = \frac{2\pi}{\lambda}(n-1)l$, represented by the unitary operator $\hat{U}[\varphi(n)]$, and experiences attenuation characterized by the virtual beam splitter $\hat{B}(T)$. Here, T signifies the transmission coefficient, l represents the length of the sample, n denotes the refractive index of the sample, and λ corresponds to the wavelength of the incident light.

Subsequent to the initial beam splitter$\hat{B}_{1/2}$, the state can be expressed as$|\psi_{in}\rangle = |ECS\rangle \otimes |0\rangle_{ae} \otimes |0\rangle_{be}$, with the subscript e indicating the ambient mode. The density matrix of this state is given by $\hat{\rho}_{in} = |\psi_{in}\rangle\langle\psi_{in}|$. The transformation of $|\psi_{in}\rangle$ through the phase shifter, virtual beam splitter, and the 50-50 beam splitter is represented by the operator $\hat{M} = \hat{B}_{1/2}\hat{B}_a(T)\hat{B}_b(T)\hat{U}(\varphi)$. By tracing out the ambient mode, the output state of the MZI is obtained as

$$\hat{\rho}_{out} = Tr\left(M\hat{\rho}_{in}M^{\dagger}\right) = |N_\alpha|^2\left\{\begin{array}{l} |\alpha'\rangle_\alpha |i\alpha'\rangle_{bb}\langle i\alpha'|_\alpha\langle\alpha'| + \left|i\alpha' e^{i\varphi}\right\rangle_\alpha \left|\alpha' e^{i\varphi}\right\rangle_{bb}\left\langle\alpha' e^{i\varphi}\right|_\alpha \left\langle i\alpha' e^{i\varphi}\right| \\ +e^{-R|\alpha|^2}\left(|\alpha'\rangle_\alpha |i\alpha'\rangle_{bb}\left\langle\alpha' e^{i\varphi}\right|_\alpha \left\langle i\alpha' e^{i\varphi}\right| + H.c.\right)\end{array}\right\}, \tag{1}$$

where simplified parameters $\alpha' = \alpha\sqrt{T/2}$ and $R = 1 - T$ is the reflection coefficient or photon loss rate.

Equation (1) shows that the non-diagonal part (representing coherence) is obviously suppressed by the photon loss, thus de-coherence is inevitable. Signal intensities of one output port can be expressed as $I = \langle\hat{n}\rangle = |N_\alpha|^2 TN\left(1 - e^{-N}\sin\left(\frac{2\pi}{\lambda}(n-1)l\right)\right)$. Resolution of ID signal can be approximately characterized by the period $\Delta n_I = \lambda/l$ of the interferometric signal, which is in agreement with the results in Ref. [13], and the resolution is not improved at all.

3 Parity detection and derivation of measurement model

Building on the insights from the existing literature, we present a quantum-based approach, specifically parity detection, to construct the output signal. This method not only enhances the resolution and sensitivity of refractive index measurements but also achieves a performance that is N times superior to conventional coherent state techniques.

Initially proposed by Bollinger[21] and subsequently implemented in phase measurements by Gerry[22], parity detection operates via a parity operator $\hat{\Pi} = e^{i\pi\hat{N}}$. This operator categorizes photon counting data {r, m} into binary outcomes ±1 based on whether the photon number N at the output ports is even or odd. Specifically, if N is even, $\Pi = +1$, otherwise $\Pi = -1$. We then project the output states $\hat{\rho}_{out}$ onto the two-mode Fock states $|r,m\rangle$.

In accordance with equation (1), the joint conditional probability $P(r,m) = \langle r,m|\hat{\rho}_{out}|r,m\rangle$ for detecting r photons at output port a and m photons at output port b can be calculated as

$$P(r,m) = |N_\alpha|^2\left\{2e^{-2|\alpha|^2}|\alpha'|^{2(m+r)}/(r!m!) + e^{-|\alpha|^2}\left[\left(-i|\alpha'|^2 e^{-i\varphi}\right)^r\left(i|\alpha'|^2 e^{-i\varphi}\right)^m/(r!m!) + H.c.\right]\right\}, \tag{2}$$

The conditional probability P(±1), obtained by summing over the photon counts corresponding to either even or odd photon numbers at one of the output ports, is given by:

$$P(\pm1) = \sum_{r,m}^{even/oddn} P(r,m) = \frac{1}{2} \pm |N_\alpha|^2\left[e^{-TN} + e^{-N\left(1-T\sin\left(\frac{2\pi}{\lambda}(n-1)l\right)\right)}\cos\left(TN\cos\left(\frac{2\pi}{\lambda}(n-1)l\right)\right)\right], \tag{3}$$

Therefore, the output signal for the parity detection strategy can be expressed as:

$$\left\langle\hat{\Pi}\right\rangle = P(+) - P(-) = 2|N_\alpha|^2\left[e^{-TN} + e^{-N\left(1-T\sin\left(\frac{2\pi}{\lambda}(n-1)l\right)\right)}\cos\left(TN\cos\left(\frac{2\pi}{\lambda}(n-1)l\right)\right)\right], \tag{4}$$

this result aligns with the findings of Zhang et al[18].

Given that $\left\langle\hat{\Pi}\right\rangle = 1$ and employing the Gaussian error-propagation formula $\delta n_P = \sqrt{\left\langle\hat{\Pi}^2\right\rangle - \left\langle\hat{\Pi}\right\rangle^2}/\left|\partial\left\langle\hat{\Pi}\right\rangle/\partial n\right|$, the sensitivity can be derived as:

$$\Delta n_P = \frac{\sqrt{1 - \left\{2|N_\alpha|^2\left[e^{-TN} + e^{-N\left(1-T\sin\left(\frac{2\pi}{\lambda}(n-1)l\right)\right)}\cos\left(TN\cos\left(\frac{2\pi}{\lambda}(n-1)l\right)\right)\right]\right\}^2}}{\left|\frac{4\pi}{\lambda}|N_\alpha|^2 TNl e^{-N\left(1-T\sin\left(\frac{2\pi}{\lambda}(n-1)l\right)\right)}\left[\cos\left(TN\cos\left(\frac{2\pi}{\lambda}(n-1)l\right)\right)\cos\left(\frac{2\pi}{\lambda}(n-1)l\right) + \sin\left(TN\cos\left(\frac{2\pi}{\lambda}(n-1)l\right)\right)\sin\left(\frac{2\pi}{\lambda}(n-1)l\right)\right]\right|}. \tag{5}$$

4　Results and Discussion

Fig. 2 illustrates the super-resolving signals achieved via the ECS-PD scheme, depicted as a red solid line. For comparative purposes, the normalized ECS-ID signal curve and the CS-PD signal curve are also presented, marked by blue dashed and green dotted lines, respectively, and all curves are plotted with N=9. As evident from Fig. 2, the signal peak of ECS-PD scheme is narrower than that of ECS-ID and CS-PD schemes. This indicates that ECS-PD scheme has the narrowest full width at half maximum, thereby demonstrating the best resolution.

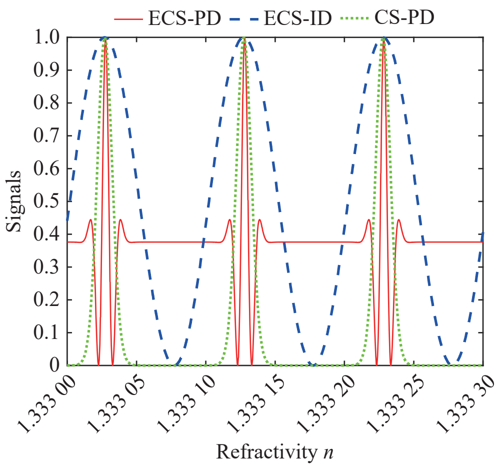

Fig. 2　Signals of the refractive index measurement system for ECS-PD, CS-PD, and normalized ECS-ID schemes.

图 2　ECS-PD, CS-PD 和归一化 ECS-ID 方案折射率测量系统信号曲线

The resolution of refractive index measurement in this work is defined as the full width at half maximum (FWHM) of the parity detection signal curve ($\langle\hat{\Pi}\rangle$ vs. refractive index n), consistent with the signal characteristics of quantum sensing (FWHM directly reflects the minimum detectable change in n).

The oscillatory behavior of $\langle\hat{\Pi}\rangle$(which determines signal periodicity and FWHM) is dominated by the cosine term $\cos\left(\mathrm{TN}\cos\left(\frac{2\pi}{\lambda}(n-1)l\right)\right)$. The signal's oscillation period Δn_{ECS-PD} (reciprocal of resolution-related frequency) is determined by the condition that the argument of the outer cosine term changes by 2π:

$$\mathrm{TN}\cos\left(\frac{2\pi}{\lambda}(n_2-1)l\right)-\mathrm{TN}\cos\left(\frac{2\pi}{\lambda}(n_1-1)l\right)=2\pi \quad , \tag{6}$$

Using the trigonometric identity $\cos A-\cos B=-2\sin\left(\frac{A+B}{2}\right)\sin\left(\frac{A-B}{2}\right)$ and for small $\Delta n=n_2-n_1$, $\sin\left(\frac{A-B}{2}\right)\approx\frac{A-B}{2}\approx\frac{\pi}{\lambda}(n_2-n_1)l$, where $A=\frac{2\pi}{\lambda}(n_2-1)l$ and $B=\frac{2\pi}{\lambda}(n_1-1)l$. Substituting these into the period condition, we obtain:

$$2TN\left|\sin\left(\frac{2\pi}{\lambda}\frac{(n_1-1)+(n_2-1)}{2}l\right)\right|\frac{\pi}{\lambda}\Delta n_{ECS-PD}l=2\pi \quad , \tag{7}$$

Simplifying (ignoring the sine term's magnitude for average period, as it varies slightly with n):

$$\Delta n_{ECS-PD}\approx\frac{\lambda}{TNl} \quad , \tag{8}$$

For the CS-PD scheme, according to Ref.[13], the signal's oscillation is dominated by a exponential term, in small-angle approximation, leading to:

$$\Delta n_{CS-PD}\approx\frac{\lambda}{l\sqrt{TN}} \quad , \tag{9}$$

Since resolution $R\propto\frac{1}{\Delta n}$ (smaller Δn indicates higher resolution), the ratio of resolutions is:

$$\frac{R_{ECS-PD}}{R_{CS-PD}}=\frac{\Delta n_{CS-PD}}{\Delta n_{ECS-PD}}=\sqrt{NT} \quad , \tag{10}$$

However, in the ideal lossless case, T (transmittance) is set to 1 for the core resolution scaling analysis. Thus, TN=N for T=1, and the FWHM of ECS-PD signal (resolution metric) scales as $1/\sqrt{N}$ relative to CS-PD, leading to the $\sqrt{N}$-fold resolution enhancement. This relationship is numerically depicted in Fig. 3, which shows the ratio of resolutions with the photon number N. The ratio of resolutions varies approximately linearly with $\sqrt{N}$.

Figure 4 illustrates the sensitivity characteristics of three detection schemes under λ = 532 nm, *l* = 5.3 mm and N = 9. The ECS-PD scheme (red solid curve) exhibits consistently enhanced sensitivity compared to the ECS-ID baseline (blue dashed line) and CS-PD approach (green dotted curve). Notably, the optimized sensitivity of the ECS-PD system achieves breakthrough performance beyond the standard noise limit (RIM-SNL), demonstrating unprecedented potential for refractive index quantification at ultralow detection thresholds.

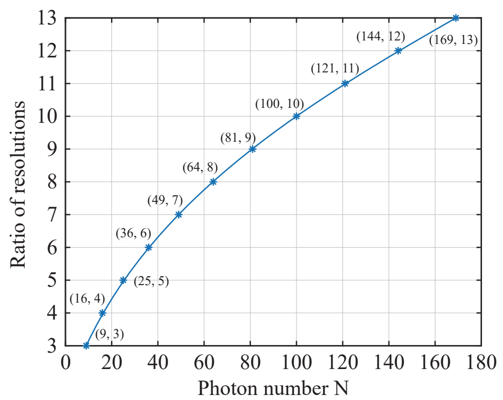

Fig. 3 Relationship between the ratio of resolutions and the photon number N.

图 3 分辨率比值与光子数 N 的关系曲线

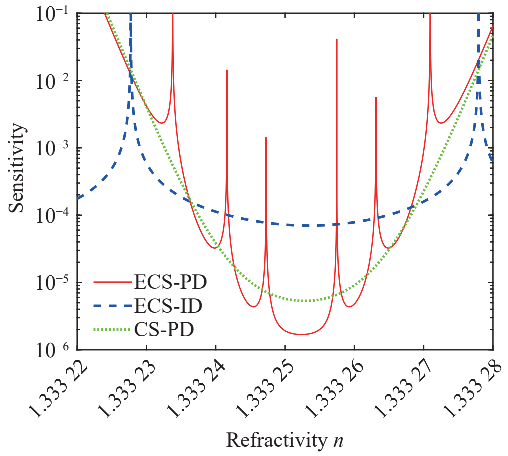

Fig. 4 Sensitivity curves of ECS-PD, ECS-ID and CS-PD schemes.

图 4 ECS-PD, CS-PD 和 ECS-ID 方案的灵敏度曲线

The quantity of photons, denoted as N, is a pivotal factor that greatly impacts on both resolution and sensitivity. Figure 5 graphically demonstrates the interplay between resolution and sensitivity as the photon number fluctuates. On this diagram, the left-hand axis signifies resolution, which is illustrated by solid lines. In contrast, the right-hand axis represents sensitivity, depicted by dotted lines. A distinct pattern emerges: with the sole exception of the ECS-ID scheme (blue line), both signal resolution and sensitivity show marked improvement as the photon number rises. Notably, the ECS-PD scheme (red line) surpasses the CS-PD (green line) and ECS-ID (blue line) schemes in terms of resolution and sensitivity, thus breaking through the classical barriers that have long constrained these parameters. It's important to highlight that the resolution of the intensity detection scheme remains impervious to changes in photon number, while its sensitivity diminishes as the photon number increases - a clear departure from the conventional CS-ID strategy. To encapsulate the findings, as the photon number grows, the ECS-PD measurement approach not only enhances resolution but also boosts sensitivity, thereby facilitating super-resolution and super-sensitivity in refractive index measurements.

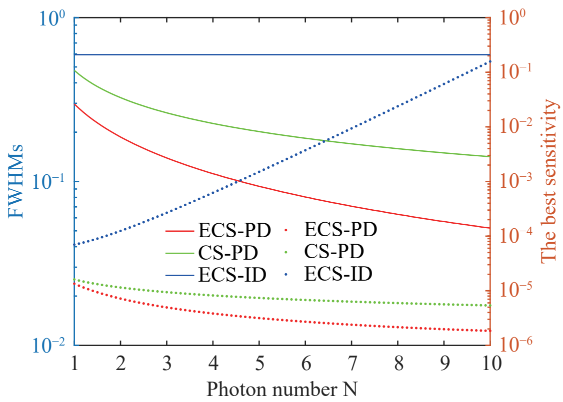

Fig. 5 Graph illustrating the impact of photon number on resolution and sensitivity.

图 5 光子数对分辨率和灵敏度的影响示意图

Figure 6 illustrates the variation of resolution with transmittance T for three distinct detection schemes across different wavelengths. The red lines correspond to the ECS-PD scheme, the blue lines to the ECS-ID scheme, and the green lines to the CS-PD scheme. It is evident that the resolutions of both the ECS-PD and CS-PD schemes diminish as losses increase (i.e., as transmittance decreases). Notably, the resolution of the ECS-ID scheme remains unaffected by losses, a fact that is also evident from the expression of the ECS-ID signal. Across the entire range of losses, the resolution of the ECS-PD scheme outperforms that of the CS-PD and ECS-ID schemes. The ECS-PD strategy transcends the traditional resolution limit. Additionally, it can be observed from the figure that all FWHMs decrease as the wavelength increases, further corroborating the inverse relationship between resolution and wavelength.

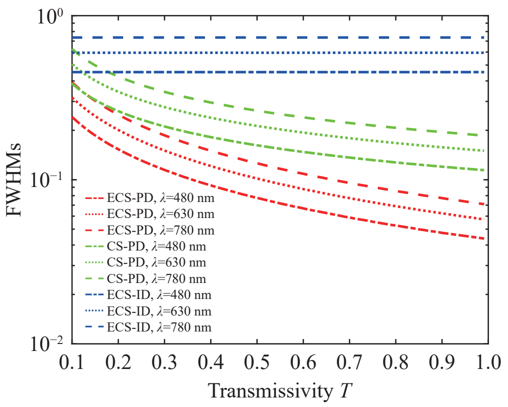

Fig. 6　Relationships between FWHM and T for ECS-PD, CS-PD, and ECS-ID schemes used different wavelengths.

图 6　ECS-PD, CS-PD 和 ECS-ID 方案在不同波长时的 FWHM 与 T 的关系曲线

Figure 7 presents the relationships between the best sensitivities and transmittance (T) for three distinct schemes. As illustrated, the sensitivity of the ECS-PD signal is inferior to that of the ECS-ID only under conditions of extremely high loss (when transmittance T is less than 0.1), but it is superior in the remaining range. When T is below 0.9, the sensitivity of CS-PD signal outperforms that of the ECS-PD, which may be attributed to the quantum decoherence of the entangled state in a lossy environment [23-24]. Quantum decoherence disrupts the coherence of the quantum system and leads to the loss of quantum information in the detected signal, ultimately diminishing the detected sensitivity. When T exceeds 0.9, the optimal sensitivity of the ECS-PD surpasses that of the CS-PD and breaks through the RIM-SNL.

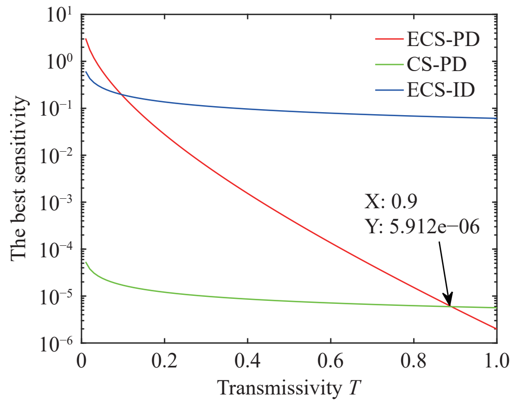

Fig. 7　Relationships between sensitivity and T for ECS-PD, CS-PD, and ECS-ID schemes.

图 7　ECS-PD, CS-PD 和 ECS-ID 方案灵敏度随 T 的变化关系曲线

5　Experimental implementation challenges

Experimental implementation of the ECS-PD scheme faces several key challenges, which may affect the predicted sensitivity and resolution. The most significant challenges and their potential impacts are summarized below.

5.1　Preparation of high-quality ECS

The ECS in our scheme is generated via interference of coherent states at a 50/50 beam splitter (Section 2.2), but experimental realization requires high coherence and stability of the input coherent states and precise control of the beam splitter ratio. Fluctuations in the amplitude$\alpha = \sqrt{N}$or phase of the input $|CS\rangle$and $|CSS\rangle$ will reduce the entanglement degree of the generated ECS. For example, a 5% fluctuation in α would decrease the off-diagonal terms of the density matrix$\hat{\rho}_{out}$ (Equation 1) by ~10%, weakening the signal contrast and increasing the FWHM (lowering resolution) by ~8–12%. A deviation of ±5% from the 50/50 splitting ratio would introduce imbalance between the $|\alpha\rangle_a|0\rangle_b$ and $|0\rangle_a|\alpha\rangle_b$ components of ECS, leading to a ~15% drop in sensitivity (calculated via Equation 5) under low-loss conditions (T>0.9).

5.2　Photon loss and decoherence

As shown in Fig. 6 and Fig. 7, photon loss (characterized by transmittance T) directly affects resolution and sensitivity. Experimental sources of loss include absorption in the sample, scattering in the optical path, and inefficiency of detectors. A loss rate of 20% (T=0.8) would reduce the $\sqrt{N}$-fold resolution enhancement to ~ $\sqrt{0.8N}$ and increase the sensitivity by ~12% (degrading performance) compared to the ideal lossless case.

Decoherence from environmental noise including thermal fluctuations or electromagnetic interference can disrupt the coherence of ECS, suppressing the oscillatory term in Equation (4). This would further broaden the signal FWHM and reduce the signal-to-noise ratio (SNR), making it harder to distinguish small changes in n.

5.3 High-precision parity detection

Parity detection relies on distinguishing even/odd photon counts at output ports, which requires low-noise photon detectors and high-speed counting and data processing. Detectors with dark counts (>10 counts/s) or quantum efficiency (<90%) would introduce errors in parity judgment. For example, a quantum efficiency of 85% would reduce the measured amplitude by ~15%, leading to a ~20% decrease in sensitivity. The ECS-PD signal exhibits rapid oscillations as a function of the refractive index n, so slow data acquisition would miss subtle changes in signal peaks, underestimating the actual resolution.

Although the experimental implementation of the ECS-PD refractive index measurement scheme faces several technical challenges, the rapid development of quantum optics, precision optical engineering and high-performance photoelectric detection technologies in recent years has made it possible to address these challenges.

6 Conclusions

This paper proposes a novel refractive index measurement scheme based on entangled coherent states and parity detection. By leveraging quantum entanglement properties to break through classical physical limits, high-precision detection is achieved. According to quantum theory, the signal and sensitivity models of ECS-ID and ECS-PD schemes are derived, simultaneously, the detected performance is analyzed and compared with the classical coherent strategy. The investigation results show that the resolution of the ECS-PD scheme is higher than the RIM-RDL and has $\sqrt{N}$ times resolution improvement relative to that of the CS-PD strategy throughout the entire loss regions. In the case of no or low loss, the sensitivity of the ECS-PD scheme exceeds the RIM-SNL and achieves ultrasensitive refractive index measurement. In conclusion, the refractive index measurement with ECS-PD scheme can break through the classical diffraction limit and the shot noise limit. The proposed scheme provides a new technical pathway for high-precision refractive index measurement.

References:

[1] CIĘSZCZYK S, SKORUPSKI K, PANAS P. Single- and double-comb tilted fibre Bragg grating refractive index demodulation methods with Fourier transform pre-processing[J]. *Sensors*, 2022, 22(6): 2344.

[2] KESAVULU C R, MONCORGÉ R, FROMAGER M, *et al*.. Electronic refractive index changes and measurement of saturation intensity in Cr^{3+} -doped YAG crystal[J]. *Optical Materials*, 2018, 78: 107-112.

[3] SHLYAGIN M G, AGRUZOV P M, PLESHAKOV I V, *et al*.. Incident-power-dependent refractive index of ferrofluid in magnetic field measured with a fiber optic probe[J]. *Optik*, 2019, 186: 418-422.

[4] ZACA-MORÁN P, PADILLA-MARTÍNEZ J P, PÉREZ-CORTE J M, *et al*.. Etched optical fiber for measuring concentration and refractive index of sucrose solutions by evanescent waves[J]. *Laser Physics*, 2018, 28(11): 116002.

[5] YAO Q H, CAO M, LIU CH. Study on measuring system of automatic image alignment refractive index based on new mathematical model[J]. *Key Engineering Materials*, 2014, 609-610: 1319-1323.

[6] PIXTON B M, GREIVENKAMP J E. Automated measurement of the refractive index of fluids[J]. *Applied Optics*,

2008, 47(10): 1504-1509.

[7] GRABNER M, KVICERA V. Measurement of the structure constant of refractivity at optical wavelengths using a scintillometer[J]. *Radioengineering*, 2012, 21(1): 455-458.

[8] LI W, ZHANG X P, ZHANG M, *et al*.. Resolving the problem of cross sensitivity in fiber Bragg grating sensor based on the principle of polarized-light interference[J]. *Frontiers of Electrical and Electronic Engineering in China*, 2007, 2(2): 234-239.

[9] ÁLVAREZ-TAMAYO R I, PRIETO-CORTÉS P. Refractive index fiber laser sensor by using a fiber ball lens interferometer with adjustable free spectral range[J]. *Sensors*, 2023, 23(6): 3045.

[10] TSAI Y J, LAROUCHE S, TYLER T, *et al*.. Design and fabrication of a metamaterial gradient index diffraction grating at infrared wavelengths[J]. *Optics Express*, 2011, 19(24): 24411-24423.

[11] NISKANEN I, SUTINEN V, THUNGSTRÖM G, *et al*.. Image information obtained using a charge-coupled device (CCD) camera during an immersion liquid evaporation process for measuring the refractive index of solid particles[J]. *Applied Spectroscopy*, 2018, 72(6): 908-912.

[12] HIRAI A, HORI Y, MINOSHIMA K, *et al*.. A bilateral comparison of optical glass refractive index between NMIJ and INRiM for the validation of the measuring systems[J]. *Metrologia*, 2012, 49(3): 283.

[13] 王强, 王倩倩, 王振, 等. 奇偶探测超分辨率折射率测量的理论研究[J]. 中国光学 (中英文), 2023, 16(2): 434-446.
WANG Q, WANG Q, WANG ZH, *et al*.. Theoretical investigation on super-resolution refractive index measurement with parity detection[J]. *Chinese Optics*, 2023, 16(2): 434-446. (in Chinese).

[14] ZHANG Y M, LI X W, YANG W, *et al*.. Quantum Fisher information of entangled coherent states in the presence of photon loss[J]. *Physical Review A*, 2013, 88(4): 043832.

[15] JING X X, LIU J, ZHONG W, *et al*.. Quantum fisher information of entangled coherent states in a Lossy Mach—Zehnder interferometer[J]. *Communications in Theoretical Physics*, 2014, 61(1): 115-120.

[16] PEZZÉ L, SMERZI A. Entanglement, nonlinear dynamics, and the Heisenberg limit[J]. *Physical Review Letters*, 2009, 102(10): 100401.

[17] 付兴丽, 冯杰, 范晓辉, 等. 基于最小偏向角法的高精度液体折射率测量装置的优化设计与测量研究[J]. 中国光学 (中英文), 2022, 15(4): 789-796.
FU X L, FENG J, FAN X H, *et al*.. Optimization design and test of a high-precision measuring device of liquid refractive index based on the method of minimum deviation angle[J]. *Chinese Optics*, 2022, 15(4): 789-796. (in Chinese).

[18] ZHANG Y M, LI X W, YANG W, *et al*. . Quantum Fisher information of entangled coherent states in the presence of photon loss[J]. *Physical Review A*, 2013, 88(4): 043832. **(查阅网上资料, 本条文献与第 14 条重复, 请确认)**.

[19] BOTO A N, KOK P, ABRAMS D S, *et al*.. Quantum interferometric optical lithography: exploiting entanglement to beat the diffraction limit[J]. *Physical Review Letters*, 2000, 85(13): 2733-2736.

[20] SILDOJA M, MANOOCHERI F, IKONEN E. Reflectance calculations for a predictable quantum efficient detector[J]. *Metrologia*, 2009, 46(4): S151-S154.

[21] BOLLINGER J J, ITANO W M, WINELAND D J, *et al*.. Optimal frequency measurements with maximally correlated states[J]. *Physical Review A*, 1996, 54(6): R4649-R4652.

[22] GERRY C C. Heisenberg-limit interferometry with four-wave mixers operating in a nonlinear regime[J]. *Physical Review A*, 2000, 61(4): 043811.

[23] VAN ENK S J, HIROTA O. Entangled coherent states: teleportation and decoherence[J]. *Physical Review A*, 2001, 64(2): 022313.

[24] RFIFI S, HASSOUNI Y. Robustness of entangled squeezed states versus entangled coherent states against channel decoherence effect[J]. *International Journal of Theoretical Physics*, 2017, 56(7): 2113-2121.

Author Biographies：

Hao Lili (1981—), female, born in Suihua, Heilongjiang Province, Ph.D., associate Professor, master student supervisor. She received her master degree and Ph.D. degree from Harbin Institute of Technology in 2007 and 2015 respectively, mainly engaged in the research of quantum optics, spatial optical solitons and optical control devices. E-mail: haolili0820@126.com

Wang Qiang (1980—), male, born in Baiquan, Heilongjiang Province, Ph.D., associate Professor, master student supervisor. In 2006 and 2016, he obtained master degree and Ph.D. degree respectively from Harbin Institute of Technology. He is currently engaged in research on quantum interference metrology and sensing, quantum lidar, etc. E-mail: wangqiang8035@163.com